Materials Advances

ROYAL SOCIETY OF CHEMISTRY

PAPER

View Article Online
View Journal | View Issue

Cite this: *Mater. Adv.*, 2025, **6**, 4016

Procion red dye chemically bonded PGMA microspheres towards leakage free and sensitivity improved lateral flow immunoassay†

Yunpeng Wang,[a] Xiaoru Dai,[a] Songle Wang,[a] Pragati Awasthi,[a] Wenkun Dong,[b] Dong Chen,[b] Shisheng Ling,[b] Xvsheng Qiao, *[acd] Zhiyu Wang,[a] Xianping Fan[ae] and Guodong Qian[a]

Lateral flow immunoassay strips (LFIAs) are reliable tools for point-of-care testing. However, their sensitivity is limited by the low extinction coefficient of microspheres with low dye content. To avoid these flaws, we report here a type of Procion red chemical-bonded amino-decorated poly(glycidyl methacrylate) (PGMA) microspheres through a three-step process, including a soap-free emulsion polymerization and carboxyl-functionalization, an amination, and a final colorization process. Ethylenediamine and Procion red are introduced onto PGMA microspheres with high concentrations of 10.2 N wt% and 39.1 wt%, respectively. Due to such heavy introduction of chemically bonded dyes, the molar extinction coefficient reached up to 3.28×10^{11} L mol^{-1} cm^{-1}, which significantly exceeds that of commercially used colloidal gold nanoparticles (9.44×10^{9} L mol^{-1} cm^{-1}). Based on the colored PGMA microspheres, we propose a drop casting and photo scanning protocol to find the minimum detectable particle density of the microspheres. As a result, the Procion red bonded PGMA microspheres could be easily identified with a density as low as 4.43×10^{4} particles per mm^{2}. Finally, when applied to COVID-19 antigen detection, the microspheres achieved a sensitivity of 0.025 ng mL^{-1} and exhibited broad pH (3–11) and long-term (7 months) stability and high specificity. They are better or comparable to other typical bio-label materials, such as colloidal gold nanoparticles and dye-composite polystyrene (PS) microspheres. The Procion red bonded PGMA microspheres offer several advantages for diagnosing major sudden and high-incidence diseases, facilitating rapid screening while maintaining high bio-detection sensitivity and stability without modifying the test format.

Received 13th February 2025,
Accepted 26th April 2025

DOI: 10.1039/d5ma00130g

rsc.li/materials-advances

1. Introduction

Immunoassays, such as lateral flow immunoassays (LFIAs), have become increasingly popular in point-of-care diagnostics due to their ease of use, rapid results, low cost, and portability.[1–4] The high sensitivity is predominantly related to the colorimetric biomarker signal[5] with high molar extinction coefficients (MECs) and low limits of detection (LOD). Colloidal gold-based traditional LFIAs are one of the most frequently employed techniques; however, they continue to be plagued by the low molar extinction coefficient and low detection sensitivity of Au microspheres. There have been numerous endeavors to improve the molar extinction coefficient of colloidal gold's test lines by increasing the size of colloidal gold particles[6] or employing a secondary addition of reagents strategy,[7,8] to enhance the molar extinction coefficient of colloidal gold's test lines. However, there are always side effects,[9] which bring higher background noise, since the large-sized and high-density Au microspheres exhibit weak Brownian motion, which impedes particle sedimentation.[9,10] The development of latex microspheres has provided an alternative approach, where microspheres are composed of dyes to achieve high molar extinction coefficients.[11–16] Latex microspheres have a lower density (<2 g cm^{-3}) compared to Au nanoparticles (19.32 g cm^{-3}). Consequently, the sedimentation speed of latex microspheres of the same weight is reduced.

[a] School of Materials Science and Engineering, Zhejiang University, Hangzhou 310058, China. E-mail: qiaoxus@zju.edu.cn; Tel: +86-571-87951234
[b] Assure Tech. (Hangzhou) Co., Ltd, Hangzhou 310015, China
[c] State Key Laboratory of Baiyunobo Rare Earth Resource Researches and Comprehensive Utilization, Baotou Research Institution of Rare Earths, Baotou 014030, China
[d] Longmen Laboratory of Luoyang, Luoyang 471000, China
[e] Ocean Academy, Zhejiang University, Zhoushan 316021, China

† Electronic supplementary information (ESI) available. See DOI: https://doi.org/10.1039/d5ma00130g

In comparison to Au nanoparticles (19.32 g cm^{-3}), latex microspheres have a lower density (<2 g cm^{-3}). Consequently, the sedimentation speed of the same weight of latex microspheres is lower.[17] Usually, the size of the latex microspheres may range up to 300–500 nm while maintaining low background noise.[15,18,19] The swelling method, the most prevalent approach to synthesizing latex microspheres, usually involves the introduction of dye molecules into the microspheres *via* a swelling agent, followed by agent removal, thereby entrapping the dye inside the inner microspheres. However, dye incorporation is limited by its solubility in polymers, typically yielding dye contents below 5% and swelling-method-derived dye composite microspheres often exhibit dye leakage during storage or labeling. However, dye incorporation is limited by its solubility in polymers, typically yielding dye contents below 5%.[12] Swelling-method-derived dye-composite microspheres often exhibit dye leakage during storage or labeling. The latter results from physical or chemical adsorption on the particle surface, compromising the final detection stability in point-of-care diagnostic cases.

To address the above-mentioned challenges for latex microspheres, a novel strategy, swelling-bonding methodology, has been developed, wherein dye molecules are seamlessly integrated into microspheres *via* a synergistic swelling-bonding paradigm, yielding an exceptionally high dye content of up to 180 mg g^{-1}.[15] This innovative approach leverages styrene as the primary constituent and vinyl-benzyl as a functional bonding moiety, which, despite dye content limitations, can be significantly improved by the availability of functional units for bonding. Surface covalent bonding has successfully immobilized dye molecules on particles, reducing dye leakage and maintaining the mono-dispersity of microspheres. Among various latex microspheres, poly(glycidyl methacrylate) (PGMA) microspheres exhibit superior performance in post-modification techniques due to their high density of functionalization groups, surpassing copolymer polystyrene (PS) in terms of functional monomers. Each PGMA monomer unit provides an active site, facilitating efficient surface amine modification through rapid nucleophilic reaction between epoxy groups and amino monomers. This enables robust covalent attachment of dyes *via* nucleophilic substitution, resulting in highly stable dye conjugation. The covalent PGMA–dye bonds confer exceptional stability, resisting detachment and pH changes, while achieving dye loading capacities above 70%.

This study utilized soap-free emulsion polymerization to synthesize PGMA microspheres, serving as adaptable templates for functionalization. Amino functionalization was achieved using small-molecular-weight ethylenediamine (EDA), resulting in elevated amino content. Subsequent dye loading yielded microspheres with enhanced molar extinction coefficients, which were rigorously characterized using an ultraviolet-visible spectrophotometer and elemental analysis. Subsequent dye loading yielded microspheres with enhanced molar extinction coefficients, which were rigorously characterized using ultraviolet-visible spectrophotometry and elemental analysis. The synthesized dye-loaded PGMA microspheres exhibit a dye content of 39.1 wt%, with a molar extinction coefficient of approximately 1 to 2 orders of magnitude greater than gold microspheres. This enhances detection sensitivity by one to two orders of magnitude compared to traditional gold nanoparticle-based assays and several times higher than polymer microspheres prepared by swelling methods. Ultimately, these microspheres exhibit desirable stability over time, across varying pH levels, and in different salt concentrations, with excellent sensitivity (0.025 ng mL^{-1}) in sandwich-format LFIAs for severe acute respiratory syndrome coronavirus 2 (SARS-CoV-2) testing.

2. Materials and methods

2.1. Experiments

2.1.1. Dye–PGMA bio-marker-preparation process. Dye–PGMA microspheres were synthesized through a three steps process. Firstly, PGMA microspheres were prepared through soap-free emulsion polymerization from GMA monomers. Subsequently, surface carboxyl-functionalized PGMA microspheres were obtained by surface polymerization with sodium acrylate. Secondly, ethylenediamine modification of PGMA microspheres (EDA–PGMA) was carried out by reacting ethylenediamine with PGMA microspheres. Finally, Procion red dye-loaded PGMA (Dye–PGMA) microspheres were prepared by reacting EDA–PGMA microspheres with Procion red. By adjusting the temperature, controlling the pH of the system, and regulating the reaction time, the dye was allowed to fully react with the amine groups on the EDA–PGMA microspheres. Reagents used in the preparation process and detailed preparation steps including condition control steps, sample collection and purification steps can be found in the ESI,† in the 'Chemical reagents and detailed methods' section.

2.1.2. LFIA application conjugation and test strip making process. Dye–PGMA–protein conjugates were prepared using a two-step method. Firstly, the carboxyl groups on the surface of Dye–PGMA were activated using EDC and NHS. Then, the particles were antibody-labeled by adding different concentrations of SARS-CoV-2 (mAb1) antibody. After that, Dye–PGMA–protein conjugates were sprayed onto the conjugation pad of the strips by a continuous gold-dotting machine. The test line and control line were sprayed with amounts of anti-rotavirus antibody and anti-virus antibody two on the nitrocellulose (NC) membrane and then dried. Finally, the LFIA components were assembled to obtain the LFIA strip. For the reagents used and detailed steps please refer to the ESI,† 'Chemical reagents and detailed methods' section.

2.1.3. Dye–PGMA carboxyl group titration procedure. A precise amount of 1 g of the dried Dye–PGMA microsphere powder was then dispersed in 50 mL of deionized water and stirred at room temperature for 12 hours. The pH of the solution was subsequently adjusted to 11 by adding 0.1 mol L^{-1} NaOH solution. Then a fixed volume of 50 μL of 0.02 mol L^{-1} HCl solution was incrementally added using a micropipette, and the stabilized conductivity readings were recorded by a conductivity meter after each addition. The carboxyl content of the Dye–PGMA microspheres was determined from the plateau

region of the titration curve, with detailed calculations available in the ESI.†

2.1.4. Drop-casting and scanning method. Deposit 0.7 μL of Dye–PGMA microsphere latex onto a nitrocellulose membrane at different concentrations. Subsequently, the nitrocellulose membrane was dried at 40 °C for 20 minutes. The patterns on the membrane were then scanned using an Epson Perfection V700 scanner. Finally, the scanned pattern color saturation data were obtained using Photoshop in the RGB channels.

2.2. Characterization

X-ray diffraction (XRD) measurements were conducted using a Shimadzu XRD-6000 X-ray diffractometer with Cu Kα radiation (λ = 1.5406 Å). X-ray photoelectron spectroscopy (XPS) was performed using an ZETIUM XPS spectrometer with a monochromatic Al Kα X-ray source. A scanning electron microscope (SEM, S4800, Japan) was employed to analyze the samples' surface structure and morphology. The dynamic light scattering (DLS) of the microspheres was determined to ascertain the samples' microsphere size distribution, polydispersity index (PDI) and Zeta potential using the Zeta-sizer Nano-ZS (0.3–10 000 nm). UV-Vis absorption spectra were recorded using a Hitachi U4100 UV-Vis spectrophotometer. Fourier transform infrared spectra were obtained with a Shimadzu FTIR-8900 spectrometer. The samples' elemental composition was determined using an Elementar Vario EL elemental analyzer (EA).

3. Results and discussion

The Dye–PGMA microspheres with carboxyl groups were synthesized through a three-step process (Fig. 1a). Firstly, a soap-free emulsion polymerization method was applied to synthesize the PGMA microspheres (Fig. 1a: reaction step 1). Secondly, the PGMA microspheres as a template are reacted with excess ethylenediamine to acquire EDA–PGMA (Fig. 1a: reaction step 2).

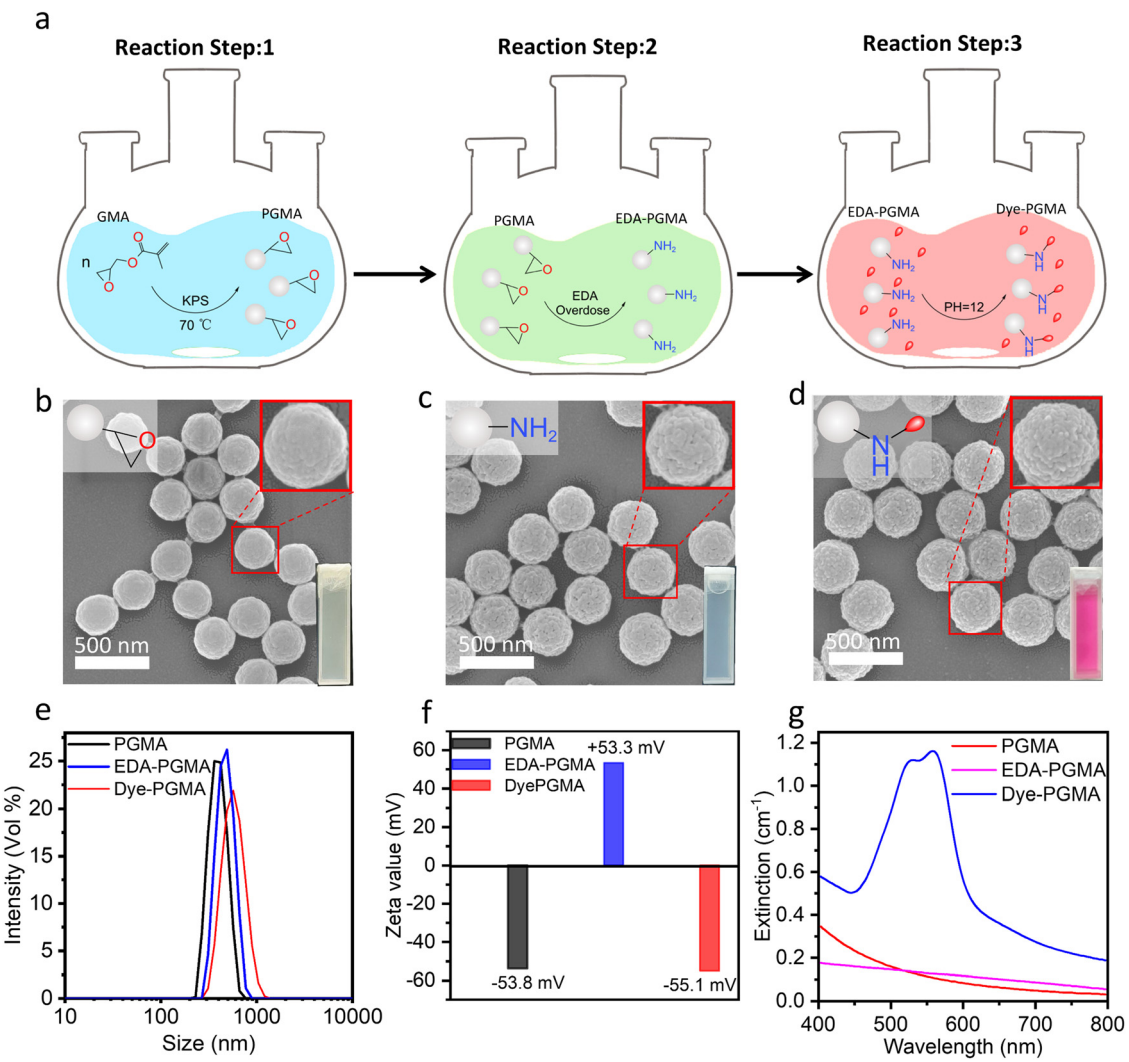

Fig. 1 (a) The synthesis steps scheme of Dye–PGMA microspheres. (b)–(g) Morphology, size, zeta potential and extinction spectra characterizations. (b)–(d) SEM images of PGMA, EDA–PGMA, and Dye–PGMA microspheres, respectively. (e) Hydrodynamic diameter distribution of PGMA, EDA–PGMA, and Dye–PGMA microspheres. (f) Zeta potential and (g) optical extinction spectra of PGMA, EDA–PGMA, and Dye–PGMA microsphere suspension.

Finally, EDA–PGMA was treated with a coloration process to obtain the Dye–PGMA (Fig. 1a: reaction step 3).

The SEM images in Fig. 1b–d exhibit the morphology and size of PGMA, EDA–PGMA, and Dye–PGMA microspheres, with the magnification image of the selected microspheres shown in the upper-right corner of each SEM image. These microspheres are well separated, with a very narrow size distribution, as observed in the SEM images and DLS data in Fig. 1e. This method resulted in Dye–PGMA microspheres with a normalized standard deviation of less than 10%. The statistical results from the SEM images and DLS data show a successive increase in microsphere size from 310 nm to 360 nm during the three-step synthesis process. This may result from the EDA and dye penetrating the microspheres and reacting with the epoxy and amino groups, increasing particle size.

As shown in the ζ-potential analysis (Fig. 1f), the absolute ζ-potential values of these three types of microspheres are all above 50 mV, showing a positive–negative–positive flip trend. The first flip is likely due to the decorated amino group on the EDA–PGMA microspheres, which can readily bind with protons (H^+) in aqueous solutions to form positively charged ammonium groups ($-NH_3^+$). The second flip is probably due to the microspheres attaching the Procion red dye colorant through the consumption of the amino groups, leading the microspheres to have a negatively charged surface. The synthesized Dye–PGMA had a sharp absorbance peak at about 562 nm with much higher absorbance than that of PGMA and EDA–PGMA microspheres at the same concentration (0.1 mg mL^{-1}). This indicates that the Procion red dye was attached to the microspheres. Further validation will be provided in the next part of the structural analysis.

The structural and chemical bonding analysis, as shown in Fig. 2, further indicated that the dye was successfully covalently bonded to the microsphere surface *via* the nucleophilic substitution reaction between the dichlorotriazine group of the Procion red dye and the amino groups on the PGMA microspheres. As shown in Fig. 2(a), the XRD pattern of the reactive red 2 dye exhibited several firm diffraction peaks, indicative of its crystalline nature. However, the synthesized microspheres, including PGMA, EDA–PGMA, and Dye–PGMA, only displayed broad amorphous humps without distinct crystalline peaks. This suggested that the dye was non-crystalline, confirming the successful incorporation of the dye in the microspheres. In Fig. 2(b), the FTIR spectra showed the disappearance of the epoxy characteristic peaks at 906 cm^{-1} and 847 cm^{-1} after amination with EDA. This indicated the successful bonding between EDA and the epoxy group from PGMA. In addition, the extinction spectra in Fig. 2(c) exhibited a red shift in the absorption peak, along with new FTIR peaks associated with the sulfonic acid group at 1068 cm^{-1} in Dye–PGMA microspheres. The Procion red dye exhibits two absorption peaks in the visible light region, with absorption peaks at 512 nm and 538 nm corresponding to the π–π* transitions of the anthraquinone group and the azo group, respectively. After chemically bonding and complexing with microspheres, a red shift in the dye's absorption peaks occurs, and the absorption baseline increases. The overall red shift of the absorption peaks is attributed to the effect of the electron-withdrawing amino group of the PGMA microspheres on the chromophores, while the increase in the absorption baseline is due to the scattering caused by the PGMA microspheres themselves. This amino electrophilic group of the EDA–PGMA reacts with the dichlorotriazinyl group in the

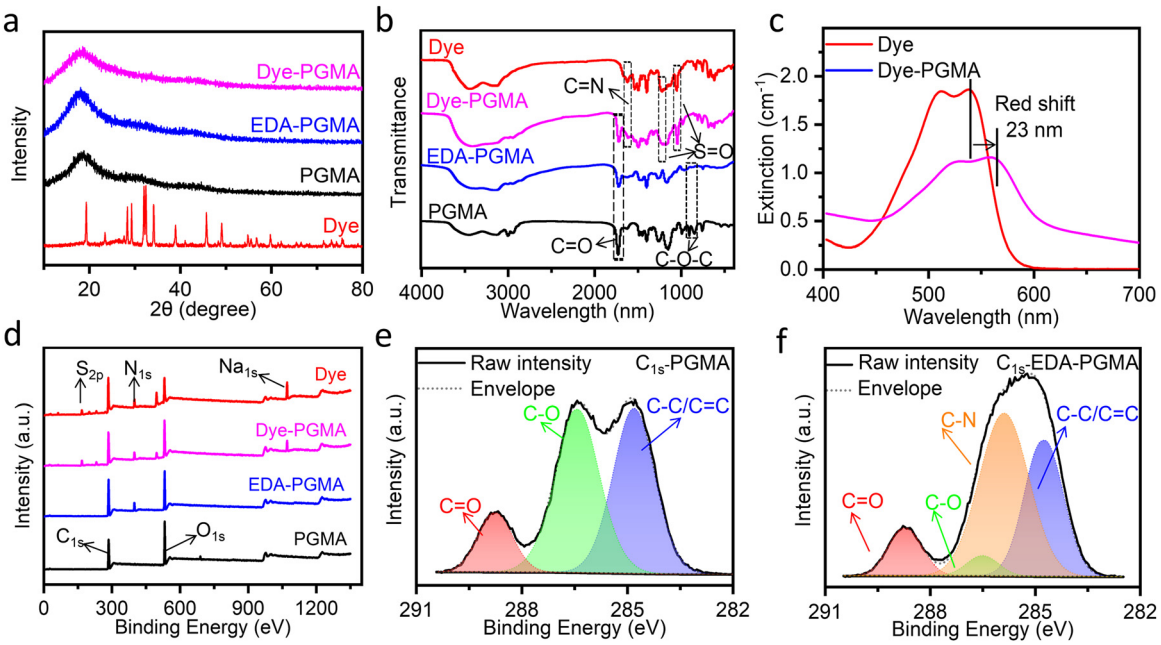

Fig. 2 (a) XRD patterns of the dried powders of PGMA, EDA–PGMA, Dye–PGMA, and Procion red colorant (Dye); (b) FT-IR spectra of the dried KBr mixtures of PGMA, EDA–PGMA, Dye–PGMA, and Dye; (c) optical extinction spectra of Dye, Dyed-PGMA, and EDA–PGMA at a concentration of 0.1 mg mL^{-1}; (d) wide-scan XPS of PGMA, EDA–PGMA, Dye–PGMA, and Dye; high-resolution XPS spectra of C1s for (e) PGMA and (f) EDA–PGMA.

Procion red molecule. The introduction of the electron-withdrawing group amino may enhance the conjugated system, extend the π-electron cloud within the molecule, and stabilize the excited state, thereby reducing the HOMO–LUMO energy gap and lowering the energy required for electron transitions. As a result, the absorption spectrum of the dye molecule undergoes a red shift, with the absorption wavelength moving towards longer wavelengths. This type of red shift, coupled with the emergence of these peaks, suggested successful chemical bonding between the dye and the EDA–PGMA microspheres.

Additionally, the XPS spectra in Fig. 2(d) show the presence of nitrogen in EDA–PGMA microspheres, and the absence of nitrogen in pure PGMA. This was also confirmed by the presence and absence of the C–N bond for EDA–PGMA and pure PGMA in the high-resolution XPS C_{1s} spectra, as shown in Fig. 2(e and f). These findings further prove the successful chemical bonding between EDA and PGMA.

In order to obtain deeply colorized Dye–PGMA microspheres, the prerequisite was achieving maximum amination of PGMA through the grafting of EDA onto the epoxy groups. The typical open-ring addition reaction of epoxy groups with amino groups is illustrated in Fig. 3(a). Under alkaline conditions, the nucleophilicity of the amino group is relatively strong. The lone pair of electrons on the amino group of EDA attacks the electrophilic carbon atom in the epoxy group of PGMA microspheres. Concurrently, the strain in the three-membered ring is relieved, and the C–O bond ruptures, forming a new carbon–nitrogen bond and a hydroxyl group (–OH). By changing the temperature from 40 °C to 100 °C, the grafting amination content varied from less than 7.0 wt% to a maximum of 9.2 wt%, and then declined to less than 7.0 wt%, as shown in Fig. S1 (ESI†). The optimal temperature for the amination grafting was revealed to be 80 °C, due to the competing reaction of water and EDA with the epoxy group on PGMA microspheres. At low temperatures, epoxy groups exhibited strong stability in the presence of water, where the reaction rate between epoxy groups and EDA was also very low. As the temperature increases, the reaction rate between EDA and epoxy groups accelerates, and water molecules surrounding the epoxy groups are gradually displaced, facilitating the penetration of EDA into PGMA microspheres. Temperature increases initially enhance amination due to increased ethylenediamine-epoxy group reactivity. However, excessive temperature increases promote epoxy group hydrolysis, impeding the comprehensive EDA reaction and reducing the final degree of amination. In this case, the maximum amination grafting ratio is 80 vol%, as evaluated with the nitrogen elemental analysis data in Fig. 3(b). Subsequently, by continuously adding EDA at 80 °C, the maximum grafting of amination reached up to 10.2 N wt%, as displayed in Fig. 3(b).

The above amination grafting protocol allows for manipulation of the dye content and color saturation in subsequent amino-dye loading processes. The particle size increased from 314.4 nm to 359.8 nm as a result of the dye molecules penetrating and expanding the microsphere, as illustrated in Fig. 1(b–d) in conjunction with the amination and dye incorporation processes. As the amination grafting ratio increases, as shown in Fig. 3(c), the incorporated dye reaches its maximum of 39.1 wt% at the amination ratio of 80 vol% EDA. Optical extinction results in Fig. 3(d) confirmed that high EDA content amination led to high EDA-decorated PGMA, resulting in a high extinction value due to the high Procion red bonding

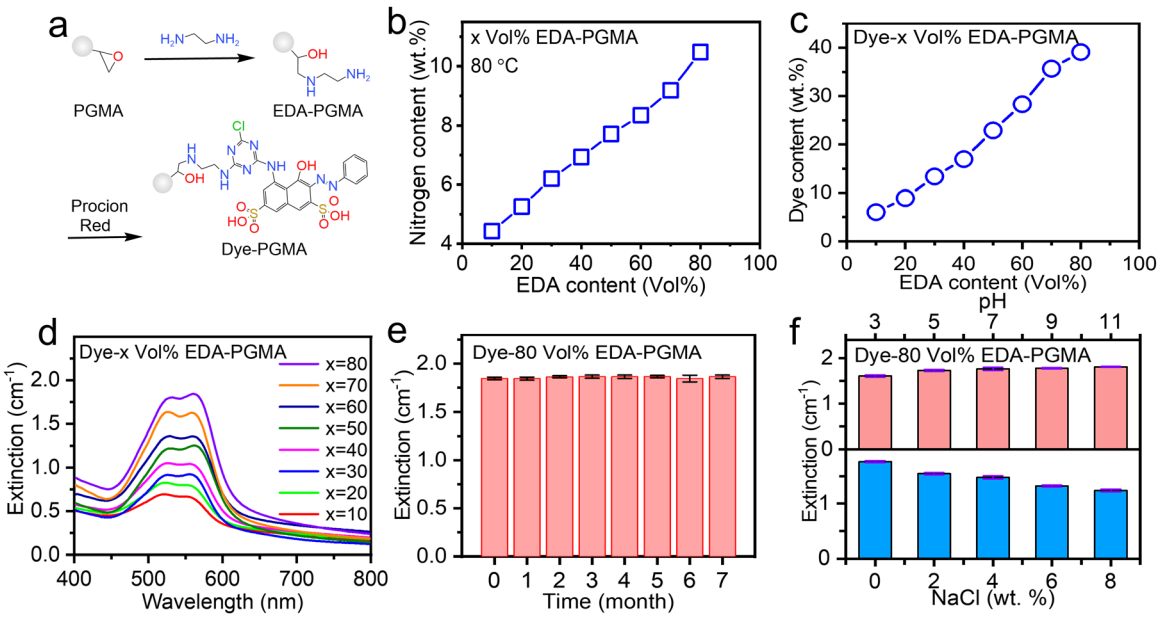

Fig. 3 Optical extinction spectra of Dye–PGMA microspheres. (a) Schematic representation of ethylenediamine (EDA) amination PGMA microspheres and later dying principle. (b) Nitrogen content of EDA–PGMA with different volume ratios of EDA. (c) Procion red dye content in Dye colored EDA–PGMA with different nitrogen contents. (d) Optical extinction spectra of Dye–PGMA microspheres in DI water (0.1 mg mL^{-1}). (e) Long term stability of the Dye–PGMA coloration in aqueous solutions. (f) PH and NaCl concentration dependent coloration stability of the Dye–PGMA in aqueous solutions.

content, where the intense blue-green extinction caused the displayed supplementary color of deep red. Based on the optimal coloration performance of the dye-loaded microspheres, we tested the Dye–PGMA extinction stability over time, pH, and NaCl concentration variations.

The results in Fig. 3(e) showed that the optical extinction remained almost unchanged at $\sim$1.80 cm^{-1} (>95%) over 7 months. With a pH variation test and a NaCl salt concentration variation test, as shown in Fig. 3(f), the optical extinction exhibited a slight increase to $\sim$1.80 cm^{-1} and a decrease to 1.25 cm^{-1}, respectively. These results evidenced that the Dye–PGMA microspheres exhibited excellent chemical stability without obvious dye leaching. The covalent bonding mechanism offers substantial advantages over adsorption and encapsulation strategies to load dye onto microspheres. Firstly, covalent bonding forms stable chemical bonds, firmly anchoring the dye to the interior or surface of the microspheres. This bond is less affected by environmental factors such as solvent, pH, or ionic strength, ensuring higher stability. In contrast, the encapsulation strategy relies on hydrophobic interactions and the physical structure of the microspheres. The adsorption strategy depends on weak forces such as van der Waals interactions, hydrogen bonds, or electrostatic attraction. Both approaches suffer from weaker binding forces, leading to leakage or desorption. Secondly, covalent bonding enables precise control over the dye's binding sites, ensuring a uniform distribution and preventing dye accumulation or non-uniformity caused by physical diffusion or electrostatic interactions. In contrast, dye distribution in encapsulation is influenced by the swelling and diffusion of the microspheres, which may lead to higher concentrations at the outer layers and lower concentrations within the core. Similarly, the adsorption method is more susceptible to local rearrangement or uneven dye distribution due to fluctuations in the solvent environment. Thirdly, dyes covalently bonded to microspheres exhibit exceptional environmental tolerance, maintaining stability even under extreme pH or high salt conditions. Encapsulation and adsorption strategies are more prone to dye release or detachment under prolonged use or harsh conditions. Covalent bonding, in addition to guaranteeing superior dye fixation stability, also enables the precise regulation of the dye release rate, thereby providing a broader range of applications in areas such as fluorescent labeling, biological detection, and durable coatings. Compared to preparing PS composite microspheres *via* the swelling method, the interaction between oil-soluble molecules and PS primarily involves van der Waals forces. For instance, as reported in the literature, the interaction energy between Nile red and PS ranges from 100 to 200 kJ mol^{-1}.[20] In our study, besides the van der Waals interactions between the dye molecules and PGMA, there are also C–N chemical bonds between the dye molecules and PGMA microspheres, with a bond energy of 274.5 kJ mol^{-1}. As a result, it is complex for the dye molecules to dissociate from the particles in an aqueous solution due to the thermal vibrations of water molecules (kBT $\sim$26 meV). This results in stronger binding between the dye and the microspheres. As a result, the Procion red dye on the surface of the particles is less likely to detach, leading to dye-composite PGMA microspheres exhibiting better resistance to desorption and enhanced stability.

Dye–PGMA color depth was characterized by a drop-casting and scanning method. Fig. 4(a) illustrates the experimental scheme, where 0.7 μL of the samples were spotted on the nitrocellulose (NC) membrane with a micropipette. After drying, the Dye–PGMA microsphere patterns on NC membranes were scanned and identified in the images in Fig. 4(b) with rose-red colors. As a result, the patterns showed a series of gradually deepened colors either with increasing Dye–PGMA microsphere number density (0.019–2.480 million particles per mm^2 from bottom to top) or with increasing the dye (Procion red) content (10–80 vol% from left to right). The Dye–PGMA microspheres displayed an apparent power function ($y = x^n$) relationship, as shown in Fig. 4(c), where the vertical y stands for RGB intensity and x stands for the Dye–PGMA microspheres concentration per square millimeter. This facilitates the establishment of a correlation between the density of Dye–PGMA microspheres, the RGB intensity, and the LOD (Fig. 4(d)). This investigation focuses on latex particle material construction over controlling these variables. The positive correlation between number densities and spot colors can be developed as a quantitative law to predict the limit of detection (*i.e.* sensitivity) for precise strip tests in colorimetric LFIAs. For this purpose, we directly employ the RGB mode, widely utilized in most computer or cell phone systems, to obtain the RGB intensities of the scanned spots. Red, green and blue intensities are determined from the difference between the computer R/G/B channel values and the blank reference NC membranes without any microspheres drop-cast. Since Dye–PGMA has extinction bands between 510–570 nm, the blue channel (B) intensity shows the best linear correlation with the Dye–PGMA microsphere number density. For simplicity, the B channel intensity is finally used to represent the spot RGB intensity. In Fig. 5(c), we plot the RGB intensities as a function of the microsphere number densities in a double-logarithmic coordinate, where the plots demonstrate a strong linear dependence on the particle number density, N_D. A detailed analysis is included in the ESI† in Fig. S2 and Table S1. Theoretically, the spot RGB intensity, I_B, is proportional to the number density, N_D, and the dye content C through the relationship of $I_B = kC^{\alpha}{\cdot}N_D$, where k is a proportional coefficient. It thus helps us to determine the minimum of microsphere number density, $N_{D\text{-}MIN} = 3{\cdot}(kC^{\alpha})^{-1}$, by setting the LOD as an RGB intensity of 3 (the dashed-dot line labeled in Fig. 4(c)).

A linear fit was obtained, under vertical logarithmic coordinates, between dye content and LOD, as shown in Fig. 5(d). The fitting slope α is -0.5, where such a linear relationship would be helpful in the practical LFIA applications. With increasing dye content from 6.0% to 39.1%, the required Dye–PGMA microsphere particle density (LOD values) could be reduced from 0.116 million particles per mm^2 to 0.443 million particles per mm^2. The light extinction performance is directly related to the absorption cross-section of individual Dye–PGMA microspheres. The higher the dye content, the larger the absorption cross-section of the Dye–PGMA microspheres. When particles

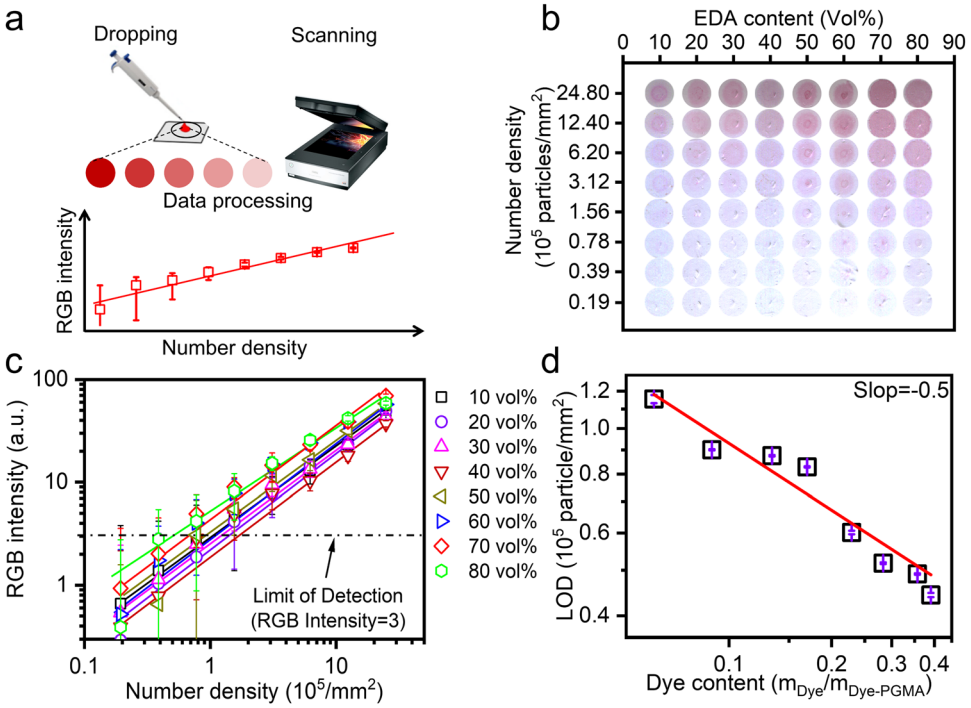

Fig. 4 (a) Schematic colorimetric assessment drop-casting method procedure of Dye–PGMA with different Dye contents on the NC membrane. (b) Drop-casting method acquired image of Dye–PGMA on the NC membrane. (c) Collected RGB intensity data from colored spots in (b). (d) Dependence of particle density at the limitation of detection (LOD) on dye content in PGMA.

of a particular concentration are placed on an NC membrane, the stronger the microspheres' light absorption capacity, and the greater the light absorption in the areas where the microsphere is present. This results in a higher contrast between the particle and blank regions, enhancing the color display effect. Therefore, the higher the dye loading on the particles, the lower the LOD exhibited by the microspheres. The sample with the highest dye content exhibits the lowest LOD of 0.044 million particles per mm^2. Although the colorimetric capability of the drop casting particles can be well related to particle density and reflected in the LOD, the homogeneous particle distribution during drop casting should be strictly controlled to fulfill the prerequisites for smooth flow (within 180 s) through a nitrocellulose (NC) membrane. On the one hand, a much larger pore size or thicker NC membrane will significantly diminish the light absorption of embedded particles, resulting in an absorption shielding effect and deteriorating LODs. If the NC membrane thickness is increased, this shielding effect intensifies, requiring a higher particle concentration to achieve the minimum distinguishable color intensity, thereby deteriorating the LOD. If the pore sizes of the NC membrane are increased, it will provide larger void space, weaken overall light scattering and deteriorate LOD values. On the other hand, the dispersion uniformity of particles on NC membranes also seriously influences LODs. Given that the particle size is approximately 360 nm, as described by Mie scattering theory, light scattering will lead to a lower LOD when non-uniform distribution occurs. Additionally, capillary action or Brownian motion drives particle movement to form a circular deposition pattern, such as with a Poisson distribution. This will lead to inhomogeneous dispersion of PGMA microspheres. Therefore, in this work, to ensure colorimetric capability, the NC membranes should be standardized with a defined pore size (15–20 μm) and a thickness of 100 μm, while particle uniformity should be obtained through ultrasonic treatment before use and a low sample volume (0.7 μL) was applied to minimize diffusion. These optimized approaches eventually promise us a more accurate estimation of the LOD. We thus established the dye content adjustment method and the relationship between dye content in Dye–PGMA microspheres and its coloration performance on the NC membrane. It supports the strip with the highest dye content and eventually achieves high sensitivity.

The Dye–PGMA microspheres were carbonylated with sodium acrylate and coupled to mAb1 to fulfill the final LFIA application requirements. Fig. 5(a) shows the titration test curve, obtained using the HCl conductivity titration method,[21] to evaluate the carboxyl content of the microspheres. The titration platform in the image, marked by a red background, represents the carboxyl group reaction signal.

The left (green background) portion of the curve illustrates the decrease in conductivity that results from the neutralization reaction between H^+ and OH^-, whereas the right (green background) portion of the curve is the result of the accumulation of H^+ in the solution after all carboxyl groups have already been used up. Then, a carboxyl content of 102 μmol g^{-1} was determined, which was deduced from the amount of HCl used during the platform stage (a detailed calculation process is supplied in the ESI,† in Fig. S3). This carboxyl concentration

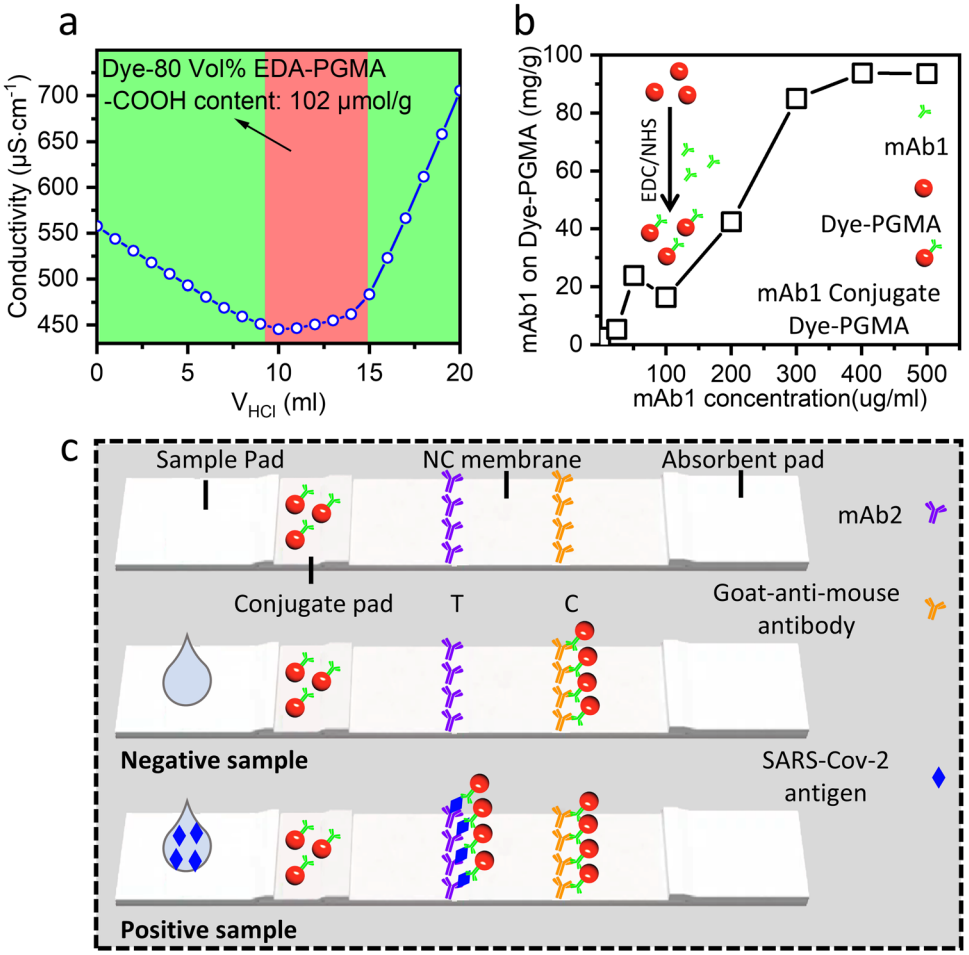

Fig. 5 (a) Titration test curve to evaluate carboxyl group content in Dye–80 vol% EDA–PGMA microspheres. (b) The effective residual SARS-Cov-2 mAb1 is charactered on the Dye–PGMA microsphere after the coupling process and shows a dependence with the nominal SARS-Cov-2 mAb1 concentration. (c) Schematic diagrams to show how the Dye–80 vol% EDA–PGMA microsphere is applied as SARS-Cov-2 antigen LFIA test strips.

is reasonable and similar to the level of approximately 100 μmol g^{-1} in commercial PS, making it suitable for use as an LFIA bio-labeling material in Dye–PGMA microspheres. Next, the carboxyl groups on the microspheres were activated using EDC/NHS, and then coupled to mAb1. Using the bicinchoninic acid (BCA) protein assay, the Dye–PGMA microspheres exhibited good protein coupling performance, as shown in Fig. 5(b), where the mAb1 coupled to Dye–PGMA microspheres increased approximately linearly with the addition of mAb1 up to 300 μg mL^{-1}, and the coupled mAb1 reached its maximum when the mAb1 concentration increased to 500 μg mL^{-1}. The maximum mAb1 conjugation rate is approximately 10 wt% of dye-microspheres. The good conjugation results indicate EDC/NHS successfully activated the carbonyl group to form the active ester, which is easier to react with the amino group on the mAb1. This could support Dye–PGMA microspheres in achieving good performance for LFIA *in vitro* diagnostic applications.

Subsequently, we fabricated an LFIA strip by incorporating the 39.1 wt% dye-loaded PGMA microspheres for SARS-CoV-2 *in vitro* diagnostic applications. According to the double-antibody sandwich LFIA scheme depicted in Fig. 5(c), the LFIA device consists of several overlapping components, including the sample pad, NC membrane, conjugate pad, and absorbent pad. mAb1-coupled Dye–PGMA microspheres are pre-immobilized on the conjugate pad, the second monoclonal antibody (mAb2) is pre-immobilized on the T ("Test") line of the NC membrane, and the goat-anti-mouse antibody is pre-immobilized on the C ("Control") line of the NC membrane. The analyte can be captured between the two complementary antibodies (capture antibody (mAb1) and detector antibody (mAb2)) resulting in a detectable signal at the T line that shows red. There are also some microspheres without capturing analytes, which can reach the C line to show a red color. Two red lines thus indicate a positive result. In contrast, a negative result would only display a single red C line, since the absence of the analyte makes the mAb1 unable to capture the Dye–PGMA microspheres, but the goat-anti-mouse antibody on the C line can still bind to them.

According to the above LFIA strip fabrication protocol, we demonstrated *in vitro* detection of SARS-CoV-2 with good sensitivity and specificity. It took 15 minutes to complete the entire detection procedure. As shown in Fig. 6(a), where the

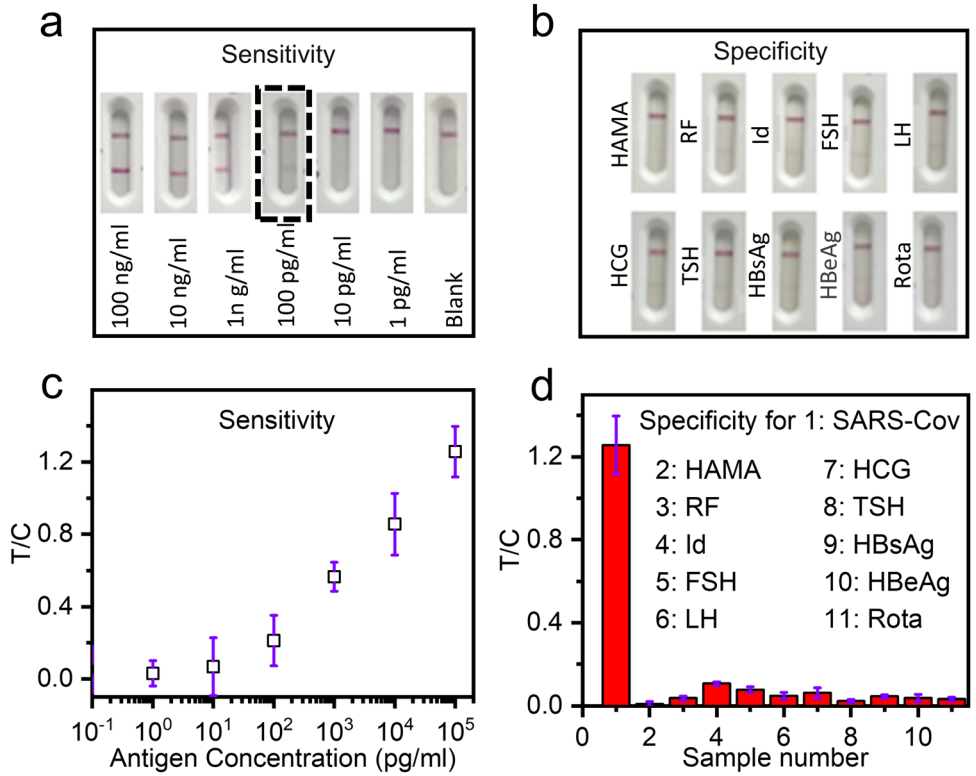

Fig. 6 The sensitivity and specificity of LFIA analysis with the Dye–80 vol% EDA–PGMA microsphere based LFIAs: (a) and (c) the sensitivity test across varying concentrations of the SARS-CoV-2 antigen and (b) and (d) specificity assessment cross-reaction results to detect the SARS-CoV-2 antigen over 10 other mycotoxins.

T lines and the C lines are located at the top and bottom of the strip, the visible detection sensitivity is 0.1 ng mL^{-1}. With the aforementioned RGB intensity method (Fig. 4(a)), the precise T/C intensity ratio was determined as shown in Fig. 6(b), where the SARS-CoV-2 antigen sensitivity is 0.025 ng mL^{-1} (three times the background noise signal). Fig. 6(c) shows the results of detecting nine types of other mycotoxins (HAMA, RF, Id, FSH, LH, HCG, TSH, HbsAg, HBeAg, and Rota). The figure shows that the T lines showed no red color, indicating no cross-reaction of the employed mAb1 and mAb2 for SARS-Cov-2 with the nine other mycotoxins. Fig. 6(d) shows the T/C bar chart, where the T/C RGB intensity ratio of detecting SARS-CoV-2 antigens reaches as high as 1.2. That is far higher than those of other mycotoxins (<0.2). Therefore, the fabricated strip with the Dye–PGMA microspheres exhibits promising *in vitro* detection specificity. The reliability was evaluated for inter-sample and intra-sample Dye–PGMA microsphere sample sets, as shown in Fig. S4 and Table S2 (ESI†). All sensitivity results were less than 0.1 ng mL^{-1} and the coefficient of variation (C_V) values for inter-samples' T/C was 3.3%, while those for the intra-samples T/C was 2.8%. These results indicate that the Dye–PGMA-based LFIA possesses high reliability. Furthermore, the detection accuracy was evaluated by assessing 10 positive serum samples at different concentrations, as shown in Fig. S6 and Table S3 (ESI†) (1000-fold). At a dilution factor much higher than the actual usage dilution, the positive detection rate reached 100%. Ultimately, we contrasted the proposed Dye–PGMA-based LFIA with the widely utilized colloid-based LFIA. By comparing detection sensitivity, specificity, detection limit, background noise, and reaction time, it was found that the Dye–PGMA microsphere-based LFIA exhibits either a considerable or much better performance than the commonly used colloidal Au method.

LFIA strips based on Procion red chemically bonded PGMA microspheres demonstrated comparable or superior *in vitro* detection performance to those based on colloidal gold nanoparticles or dye-swollen PS microspheres, especially with better color depths and detection sensitivities. The use of Procion red reactive red dyes enabled PGMA to achieve a dye loading capacity of up to 39.1 wt%, 4 to 5 times higher than that of dye composite PS microspheres through swelling methods. This is mainly attributed to the EDA (up to 10.2 wt% by N%) highly functionalized PGMA microspheres as an aminated template. The molar extinction coefficient of Procion red chemically bonded PGMA microspheres reached 3.28×10^{11} L mol^{-1} cm^{-1}, which is 34.75 times that of 40 nm colloidal gold (9.44×10^{9} L mol^{-1} cm^{-1}). This is mainly attributed to the high dye-loading capacity of the reactive red dye on PGMA, which reaches 39.1 wt%, and the high absorption cross-section of 1.25×10^{-9} cm^2 of the microspheres. This high concentration of reactive red dye loading allowed the PGMA microsphere particle density to be minimized to as low as 4.43×10^4 particles per mm^2 when applied to nitrocellulose membranes. It is two orders of magnitude more sensitive than commercial

Table 1 Comparison of dye concentration (C_{DYE}), molar extinction coefficient, particle density limitation of detection (LOD), and bio-detection sensitivity (the SARS-CoV-2 antigen) among the microspheres in this work and other typical bio-markers of LFIA

Material	C_{DYE} (mmol g^{-1})	ε (L mol^{-1} cm^{-1})	LOD (particles per mm^2)	Sensitivity (ng mL^{-1})	Ref.
Colloidal gold NPs	—	9.44×10^9	3.78×10^6	62.5	9,15
PDA NPs	—	2.88×10^{10}	—	1.51	22,23
Dye-PS microspheres	0.44	3.47×10^{10}	—	0.415	15
Dye–PGMA microspheres	1.59	3.28×10^{11}	4.43×10^4	0.025	This work

gold colloids. When applied to sandwich-type bio-detection strips for SARS-CoV-2, the detection sensitivity was less than 0.1 ng mL^{-1}, approximately two orders of magnitude higher than that of colloidal gold markers.

Additionally, Procion red chemically bonded PGMA microspheres exhibited superior stability compared to colloidal gold and dye-swollen PS microspheres, retaining over 95% of the extinction performance after 7 months. The binding energy of the C–N chemical bond between the reactive red dye and PGMA microspheres is stronger than the van der Waals interactions between dye and microspheres with the swelling method. This directly induces superior dye leakage resistance and stable extinction performance of the chemically bonded PGMA microspheres. Eventually, Procion red chemically bonded PGMA microspheres are excellent *in vitro* detection marker materials with their outstanding color depth, detection sensitivity, and stability. They provide promising new material for developing high-sensitivity LFIA strips with low detection limits and will promote significant advances of immunoassay testing (Table 1).

4. Conclusion

In summary, a three-step method was developed to synthesize stable and high dye-content composite PGMA microspheres and apply them to the sandwich-form LFIA as the biomarker. Carboxyl groups were grafted onto the surface of PGMA microspheres through a soap-free emulsion polymerization method, achieving carboxyl functionalization (102 μmol g^{-1}). Amino functionalization was then performed by reacting the epoxy groups in PGMA with an excess of ethylenediamine, resulting in a high nitrogen content of up to 10.2 wt%. Using a chemical bonding method, Procion red dye was incorporated into highly amino-functionalized PGMA microspheres with a high loading ratio (39.1 wt%) to show a high extinction coefficient (3.28×10^{11} L mol^{-1} cm^{-1}) and excellent chemical stability. The quantitative measurement of the RGB color depth was proposed for the PGMA microspheres using a drop-casting and photo-scanning method. The results showed that the Procion red bonded PGMA microspheres could be well identified with a density as low as 4.43×10^4 particles per mm^2. On this basis, an LFIA for the qualitative detection of the SARS-CoV-2 antigen was demonstrated to achieve a low detection limit of 0.025 ng mL^{-1} and a reasonable bio-detection specificity. This study thus provides a new polymer composite microsphere bonded with a high content of dye molecules offering several biotesting advantages. The dye-loaded microspheres prepared by this method can also be extended to applications for diagnosing major sudden and high-incidence diseases, to achieve highly sensitive clinical point-of-care testing.

Author contributions

Yunpeng Wang: conceptualization, methodology, data analysis, and writing the original draft. Xiaoru Dai: data analysis and methodology. Songle Wang: data analysis and polishing of the original draft. Shisheng Ling, Wenkun Dong, Dong Chen: resources, methodology, supervision and funding acquisition. Pragati Awasthi, Xvsheng Qiao, Zhiyu Wang, Xianping Fan and Guodong Qian: conceptualization, methodology, project administration, investigation, supervision and writing (review and editing).

Data availability

Data generated during and/or analyzed during the current study are included in this published article (and its ESI†). Detailed reports that support the findings in this study are available from the corresponding author upon reasonable request.

Conflicts of interest

The authors declare that they have no known competing financial interests or personal relationships that could have appeared to influence the work reported in this paper.

Acknowledgements

The authors gratefully acknowledge financial support from the National Key R&D Program of China (Grant No. 2022YFB3503700), the "Leading Goose" R&D program of Zhejiang Province (No. 2022C01142), and the Collaboration Program of ZJU-Assure Research & Development Center (No. 2022-KYY-509108-0023).

References

1 F. Hou, S. Sun, S. W. Abdullah, Y. Tang, X. Li and H. Guo, The application of nanoparticles in point-of-care testing (POCT) immunoassays, *Anal. Methods*, 2023, **15**, 2154–2180.
2 X. Nan, L. Yang and Y. Cui, Lateral flow immunoassay for proteins, *Clin. Chim. Acta*, 2023, **544**, 117337.
3 Y. Liu, L. Zhan, Z. Qin, J. Sackrison and J. C. Bischof, Ultrasensitive and highly specific lateral flow assays for point-of-care diagnosis, *ACS Nano*, 2021, **15**, 3593–3611.

4 E. B. Bahadır and M. K. Sezgintürk, Lateral flow assays: Principles, designs and labels, *TrAC, Trends Anal. Chem.*, 2016, **82**, 286–306.
5 L. Zhan, S. Guo, F. Song, Y. Gong, F. Xu, D. R. Boulware, M. C. McAlpine, W. C. W. Chan and J. C. Bischof, *Nano Lett.*, 2017, **17**, 7207–7212.
6 X. Chen, L. Ding, X. Huang and Y. Xiong, Tailoring noble metal nanoparticle designs to enable sensitive lateral flow immunoassay, *Theranostics*, 2022, **12**, 574–602.
7 W. Yang, X. Li, G. Liu, B. Zhang, Y. Zhang, T. Kong, J. Tang, D. Li and Z. Wang, A colloidal gold probe-based silver enhancement immunochromatographic assay for the rapid detection of abrin-a, *Biosens. Bioelectron.*, 2011, **26**, 3710–3713.
8 D. H. Choi, S. K. Lee, Y. K. Oh, B. W. Bae, S. D. Lee, S. Kim, Y.-B. Shin and M.-G. Kim, A dual gold nanoparticle conjugate-based lateral flow assay (LFA) method for the analysis of troponin I, *Biosens. Bioelectron.*, 2010, **25**, 1999–2002.
9 B. N. Khlebtsov, R. S. Tumskiy, A. M. Burov, T. E. Pylaev and N. G. Khlebtsov, Quantifying the numbers of gold nanoparticles in the test zone of lateral flow immunoassay strips, *ACS Appl. Nano Mater.*, 2019, **2**, 5020–5028.
10 J. Li, H. Duan, P. Xu, X. Huang and Y. Xiong, Effect of different-sized spherical gold nanoparticles grown layer by layer on the sensitivity of an immunochromatographic assay, *RSC Adv.*, 2016, **6**, 26178–26185.
11 L. Fan, J. Yang, J. Wu, F. Li, W. Yan, F. Tan, M. Zhang, M. S. Draz, H. Han and P. Zhang, Deeply-dyed nanobead system for rapid lateral flow assay testing of drugs at point-of-care, *Sens. Actuators, B*, 2022, **362**, 131829.
12 J. H. Lee, I. J. Gomez, V. B. Sitterle and J. C. Meredith, Dye-labeled polystyrene latex microspheres prepared *via* a combined swelling-diffusion technique, *J. Colloid Interface Sci.*, 2011, **363**(1), 137–144.
13 J. S. Song, F. Tronc and M. A. Winnik, Monodisperse, controlled micron-size dye-labeled polystyrene particles by two-stage dispersion polymerization, *Polymer*, 2006, **47**, 817–825.
14 D. Horák, F. Švec and J. M. J. Fréchet, Preparation of colored poly (styrene-*co*-butyl methacrylate) micrometer size beads with narrow size distribution by dispersion polymerization in presence of dyes, *J. Polym. Sci., Part A:Polym. Chem.*, 1995, **33**, 2961–2968.
15 J. Li, P. Zhang, Q. Xu, Y. Nie, S. Shao, Z. Wang and Y. Jiang, Preparation of dyed polymer microspheres by a physical–chemical dual-binding method and their application in lateral flow immunoassay, *Anal. Methods*, 2024, **16**, 2033–2043.
16 F. Shi, Y. Tang, Z. H. Xu, Y. X. Sun, M. Z. Ma and C. F. Chen, Visual typing detection of brucellosis with a lateral flow immunoassay based on coloured latex microspheres, *J. Appl. Microbiol.*, 2019, **132**, 199–208.
17 V. Šmigol, F. Švec, K. Hosoya, Q. Wang and J. M. Fréchet, Monodisperse polymer beads as packing material for high-performance liquid chromatography. Synthesis and properties of monidisperse polystyrene and poly(methacrylate) latex seeds, *Angew. Makromol. Chem.*, 1992, **195**, 151–164.
18 M. Zhu, Y. Jia, L. Peng, J. Ma, X. Li and F. Shi, A highly sensitive dual-color lateral flow immunoassay for brucellosis using one-step synthesized latex microspheres, *Anal. Methods*, 2019, **11**, 2937–2942.
19 J. Liang, K. Wang, L. Gong, Z. Zhang, J. Wang, Y. Cao and H. Zeng, High extinction coefficient material combined with multi-line lateral flow immunoassay strip for ultrasensitive detection of bacteria, *Food Chem.*, 2023, **427**, 136721.
20 V. A. Tikhomirov, A. V. Odinokov, A. A. Bagatur'yants and M. V. Alfimov, Modeling the surface of polystyrene and the adsorption of dye molecules on this surface, *Theor. Exp. Chem.*, 2011, **46**, 342–349.
21 S. Liu, L. Dou, X. Yao, W. Zhang, B. Zhao, Z. Wang, Y. Ji, J. Sun, B. Xu, D. Zhang and J. Wang, Polydopamine nanospheres as high-affinity signal tag towards lateral flow immunoassay for sensitive furazolidone detection, *Food Chem.*, 2020, **315**, 126310.
22 Z. Liu, C. Cao, H. Tong and M. You, Polydopamine Nanoparticles-Based Three-Line Lateral Flow Immunoassay for COVID-19 Detection, *Biosensors*, 2023, **13**, 352.
23 J. Zhang, F. Chai, J. A. Li, S. Wang, S. Zhang, F. Li, A. Liang, A. Luo, D. Wang and X. Jiang, Weakly ionized gold nanoparticles amplify immunoassays for ultrasensitive point-of-care sensors, *Sci. Adv.*, 2024, **10**, 5698.